1989

The Uranium-Trend Dating Method: Principles and Application for Southern California Marine Terrace Deposits

Daniel R. Muhs

John N. Rosholt

Charles L. Bush

Quaternary International, Vol. 1, pp. 19–34, 1989.
Printed in Great Britain.

1040-6182/89 $0.00 + .50
Pergamon Press plc

THE URANIUM-TREND DATING METHOD: PRINCIPLES AND APPLICATION FOR SOUTHERN CALIFORNIA MARINE TERRACE DEPOSITS

Daniel R. Muhs, John N. Rosholt and Charles A. Bush
U.S. Geological Survey, MS 424, Box 25046, Denver Federal Center, Denver, CO 80225, U.S.A.

Uranium-trend dating is an open-system method for age estimation of Quaternary sediments, using disequilibrium in the ^{238}U–^{234}U–^{230}Th decay series. The technique has been applied to alluvium, colluvium, loess, till, and marine sediments. In this study we tested the U-trend dating method on calcareous marine terrace deposits from the Palos Verdes Hills and San Nicolas Island, California. Independent age estimates indicate that terraces in these areas range from ~80 ka to greater than 1.0 Ma. Two low terraces on San Nicolas Island yielded U-trend plots that have a clustered array of points and the ages of these deposits are indeterminate or highly suspect. Middle Pleistocene terraces and one early Pleistocene terrace on San Nicolas Island and all terraces on the Palos Verdes Hills gave reasonably linear U-trend plots and estimated ages that are stratigraphically consistent and in agreement with independent age estimates. We conclude that many marine terrace deposits are suitable for U-trend dating, but U-trend plots must be carefully evaluated and U-trend ages should be consistent with independent geologic control.

INTRODUCTION

Marine terraces are coastal landforms consisting of shore platforms covered by a veneer of marine sediments, commonly sands and gravels of variable thickness. Many marine terrace deposits are fossiliferous, and isotopic or chemical analyses of fossil marine molluscs and corals often allow relative or numerical age estimates to be made. Marine terraces are important landforms in that they are normally formed during eustatic high stands of sea; thus, they formed during interglacial or interstadial periods of the Quaternary. Where these landforms are found on tectonically active, emergent coastlines such as the Pacific coast of North America, they form flights of terraces that represent successive sea-level high stands superimposed on a tectonically-rising coastline.

On the California coast, marine terraces have been the subjects of intensive study over the past decade (see summaries by Lajoie, 1986 and Muhs, 1987). Marine terraces have been investigated for sea-level history and coastal tectonics (Birkeland, 1972; Bradley and Griggs, 1976; Wehmiller *et al.*, 1977; Kern, 1977; Lajoie *et al.*, 1979; Woods, 1980; McLaughlin *et al.*, 1983; Muhs, 1983a, 1985), for paleontology and paleoceanography (Kennedy, 1978; Kennedy *et al.*, 1982; Muhs and Kyser, 1987), and as frameworks for the study of coastal landform modification and soil chronosequences (Muhs, 1982; Hanks *et al.*, 1984; Crittenden and Muhs, 1986; Harden *et al.*, 1986).

Accurate age determinations of marine terraces are critical to all of the studies cited above. The most reliable method is $^{230}Th/^{234}U$ closed-system dating of fossil corals, and a number of such age estimates have been generated by this method in recent years for terrace deposits in California and Baja California (Ku and Kern, 1974; Omura *et al.*, 1979; Muhs and Szabo, 1982; Muhs *et al.*, 1987; Rockwell *et al.*, 1987; Ashby *et al.*, 1987). Uranium-series dating of fossil molluscs and sea urchins has not been successful because these materials do not form closed systems with respect to ^{238}U and its daughter products (Kaufman *et al.*, 1971; Szabo and Vedder, 1971; Muhs and Kennedy, 1985). Amino acid racemization techniques on molluscs have been important in relative age determinations, and can discriminate older marine fossils from younger fossils, but racemization kinetics are not well enough understood at present to allow numerical estimates (Wehmiller *et al.*, 1977; Wehmiller and Belknap, 1978; Kennedy *et al.*, 1982; Muhs, 1985).

Despite the recent successes of dating California marine terraces by the $^{230}Th/^{234}U$ method on fossil corals, two problems still remain: (1) corals are not found in all terrace deposits; and (2) $^{230}Th/^{234}U$ dating of corals has a range of about 5 ka to 350 ka. Thus, terraces in many areas cannot be dated by this method. These limitations preclude the generation of important data, such as long-term Quaternary uplift rates. What is needed in many studies of marine terraces is a dating method that allows age determinations of terrace deposits that lack fossil corals or that are beyond the range of $^{230}Th/^{234}U$ dating. In this study, we test the applicability of the uranium-trend dating method to southern California marine terrace deposits. We first review the principles and other aspects of the uranium-trend method (summarized from Rosholt, 1985 and Rosholt *et al.*, 1985a) and then test and evaluate its utility for dating terrace deposits on the Palos Verdes Hills and San Nicolas Island, California.

HISTORY OF URANIUM-TREND DATING

An important dating method in Quaternary geology is the $^{230}Th/^{234}U$ technique, which has been applied mainly to marine and near-surface continental carbonates. A prerequisite for successful application of this technique is that materials to be analyzed have been closed systems in a geochemical sense. However, most

Quaternary sediments and soils are characterized by open-system behavior with regard to ^{238}U and its long-lived daughter products, ^{234}U and ^{230}Th (Rosholt *et al.*, 1966). Studies of these nuclides in sediments and soils have also shown time-related patterns of isotope fractionation (Rosholt *et al.*, 1966) that provide the basis for a new, open-system method called uranium-trend dating. A preliminary model for uranium-trend dating was described by Rosholt (1980) and Szabo and Rosholt (1982) who analyzed samples from a variety of Quaternary deposits including alluvium, eolian sediments, glacial deposits, and zeolitized volcanic ash. A revised model for uranium-trend systematics was given by Rosholt (1985a). The empirical model requires time calibration based on analyses of deposits of known age; results of these calibrations are included in Rosholt *et al.* (1985a). The technique has been applied by Rosholt and Szabo (1982) to dating marine deposits on the U.S. Atlantic coastal plain where estimated U-trend ages of bulk marine sediments agreed well with conventional $^{230}Th/^{234}U$ ages of corals from the same sediments. U-trend age estimates of tills are in agreement with the relative ages and degree of soil development in these tills (Shroba *et al.*, 1983; Rosholt *et al.*, 1985a). U-trend dating has been applied extensively for development of chronologies of Quaternary alluviation in arid regions of Nevada, Utah, and Arizona. Rosholt *et al.* (1985b, 1988) dated Quaternary alluvium in the Nevada Test Site area. The estimated ages for this alluvium agree well with local stratigraphic control, degree of soil development, and independent numerical age control. In Utah, Colman *et al.* (1986) reported estimated ages of basin-fill sediments by U-trend that are in reasonable agreement with ages estimated by other methods. Rosholt *et al.* (1986) and Machette *et al.* (1986) reported U-trend age estimates for terrace alluvium along the Colorado River in Grand Canyon National Park, Arizona. These ages are in agreement with the depositional sequence of the terraces, and suggest a history of periodic downcutting and deposition in the lower part of the canyon during the Quaternary.

PRINCIPLES OF URANIUM-TREND DATING

In order to satisfy the requirements for uranium-trend dating, the distribution of uranium-series members in the geochemical environment during and after sedimentation must have been controlled by open-system behavior. Sediments and soils interact with materials carried in water that moves through these deposits. This water usually contains at least small amounts of dissolved uranium and, as this uranium decays, it produces a trail of radioactive daughter products that are readily adsorbed on solid matrix material. If the trail of daughter products, ^{234}U and ^{230}Th, is distributed through the deposits in a predictable pattern, then a model for uranium-trend dating can be developed. The large number of geochemical variables in an open system precludes the definition of a rigorous mathematical model for uranium migration. Instead, an empirical model is used to define the parameters that can reasonably explain the patterns of isotopic distribution. This model requires independent time calibration provided by deposits of known-age and careful evaluation of the stratigraphic relationships of the deposits to be dated (Rosholt *et al.*, 1985a).

In the geologic environment, uranium occurs chiefly in two different forms: (1) as a resistate or fixed form (solids are the dominant component) in which uranium is structurally incorporated in matrix minerals; and (2) as a mobile form (water is the dominant component) which includes the uranium flux that migrates through a deposit. In the ^{238}U-^{234}U–^{230}Th series, mobile uranium is responsible for the disequilibrium processes which are the basis for the uranium-trend dating technique. A fractionation process is the preferential leaching of ^{234}U from the fixed form. As a deposit undergoes interstratal or pedogenic alteration, some uranium isotopes are released and become mobile; this process results in another form of isotope fractionation caused by alpha-recoil effects.

Determinations of the abundances of ^{238}U, ^{234}U, ^{230}Th, and ^{232}Th in a single sample do not establish a meaningful time-related pattern of distribution of these isotopes in an open-system environment. However, analyses of several samples, each of which has slightly different physical properties and slightly different chemical composition, may provide a useful pattern for determining the distribution of these isotopes (Rosholt *et al.*, 1985a). Analyses of 5 to 8 samples per deposit, from numerous alluvial, colluvial, glacial, and eolian deposits have shown that such time-related patterns exist.

EMPIRICAL MODEL

Theory

The very long-lived ^{238}U isotope (half-life of 4.468×10^9 years), upon radioactive decay, produces long-lived daughter products, ^{234}U and ^{230}Th (Ivanovich, 1982). The half-life of ^{234}U is 248,000 years (Ivanovich, 1982). This isotope has a potential for use as a geochemical tracer extending over the last 900,000 years. The half-life of ^{230}Th is 75,200 years (Ivanovich, 1982). Because of its daughter–parent relation to ^{234}U, it is a key isotope used in nearly all uranium-series dating models (Ku, 1976).

For surficial deposits, the starting time for the uranium-trend clock is the initiation of water movement through the sediment rather than initiation of soil development, although both of these processes may start at essentially the same time. The uranium, thorium, and radioactive equilibrium systematics in the parent material are disturbed during transport, and new, readjusted systematics are established in the sediment at the time of deposition. One of the assumptions required by the model is that sufficient mixing occurred during transport and deposition of the sediment such that it has nearly the same original $^{234}U/^{238}U$ ratio in each sample of the deposit selected for dating.

The empirical model incorporates a key component referred to as uranium flux, F(0). The actual physical significance of F(0) is not well understood. It is related to the flux or movement of mobile-phase uranium through a deposit; theoretically, the effect of this flux on isotopic variations should decrease exponentially with time. An oversimplified example of the flux in alluvium would be the initial large volume of water that accompanies deposition followed by smaller volumes of water during compaction of the sediments and subsequent soil development. The quantity of water migrating through a deposit, its flow rate, and the concentration of uranium in this water are components of the flux; the magnitude of the flux is a function of the concentration of uranium in the mobile phase relative to the concentration of uranium in the fixed phase.

The isotopic composition (expressed in activity units) of several samples from the same depositional unit is required for solution of the model. The value from which ages are calculated is the slope of the line representing the variation from radioactive equilibrium between the following parents and daughters:

$$\frac{\Delta(^{234}U - {}^{238}U)}{\Delta(^{234}U - {}^{230}Th)}. \quad (1)$$

A related slope is

$$\frac{\Delta(^{234}U - {}^{238}U)}{\Delta(^{238}U - {}^{230}Th)}. \quad (2)$$

The two forms of slope are dependent because

$$\frac{\Delta(^{234}U - {}^{238}U)}{\Delta(^{238}U - {}^{230}Th)} = \frac{\Delta(^{234}U - {}^{238}U)}{\Delta[(^{234}U - {}^{230}Th) - (^{234}U - {}^{238}U)]} \quad (3)$$

and this form is used for a computer solution of the age (Rosholt, 1985). The terms $\Delta(^{238}U - {}^{230}Th)$ and $\Delta(^{234}U - {}^{230}Th)$ are used rather than $\Delta(^{230}Th - {}^{238}U)$ and $\Delta(^{230}Th - {}^{234}U)$ to comply with the convention used by geochronologists where the slope of an isochron increases with age. A diagram (Fig. 1) shows the hypothetical development of a U-trend slope for a three-sample profile. Changes in isotopic composition with time should ideally follow a complex radioactive growth and decay curve; the U-trend slope for the three samples is represented by the tangent to this curve.

Isotopic measurements are expressed as ratios of $^{234}U/^{238}U$ and $^{230}Th/^{238}U$; the isotopic variations in the model are normalized to ^{238}U and written in the form of the following equation (Rosholt, 1985):

$$\frac{Y}{X} = \frac{\Delta(^{234}U - {}^{238}U)/^{238}U}{\Delta(^{234}U - {}^{230}Th)/^{238}U} = \frac{C_1e^{-\lambda_0 t} + C_2e^{-\lambda_2 t}}{C_3e^{-\lambda_0 t} + C_4e^{-\lambda_2 t} + C_5e^{-\lambda_3 t}} \quad (4)$$

where

$$C_1 = \frac{-\lambda_0\lambda_2}{\lambda_2 - \lambda_0}; \quad C_2 = \frac{\lambda_2\lambda_2}{\lambda_2 - \lambda_0} - \lambda_2;$$

$$C_3 = \frac{3\lambda_0\lambda_2\lambda_3}{(\lambda_2 - \lambda_0)(\lambda_3 - \lambda_0)};$$

$$C_4 = \frac{3\lambda_2\lambda_2\lambda_3}{(\lambda_0 - \lambda_2)(\lambda_3 - \lambda_2)} + 2\lambda_2;$$

$$C_5 = \frac{3\lambda_2\lambda_3\lambda_3}{(\lambda_0 - \lambda_3)(\lambda_2 - \lambda_3)} - \lambda_3;$$

and where λ_0 is the decay constant of F(0) = ln 2/[half period of F(0)]; λ_2 is the decay constant of ^{234}U; λ_3 is the decay constant of ^{230}Th; and t is the time since deposition of the sediment. These are empirical equ-

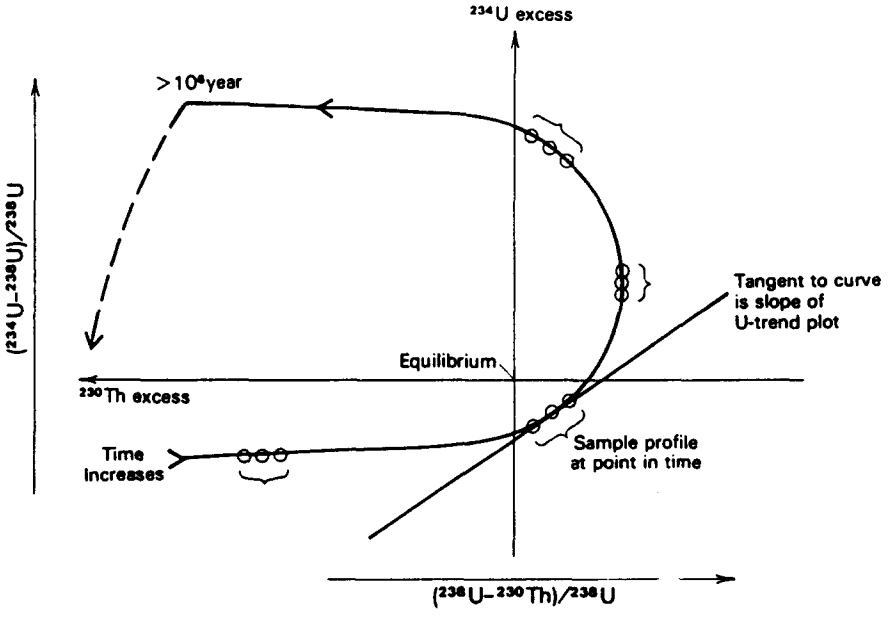

FIG. 1. Hypothetical development of ^{234}U–^{230}Th disequilibrium for U-trend slope of a three-sample deposit (after Rosholt, 1985).

ations which were determined by computer synthesis to provide a model with the U-trend ages that have the closest agreement with independently-dated deposits (Rosholt *et al.*, 1985a). To simplify calculations, we have modified Eq. 2 slightly as follows:

$$\frac{Y}{X - Y} = \frac{\Delta(^{234}U - {}^{238}U)/^{238}U}{\Delta(^{238}U - {}^{230}Th)/^{238}U} \quad (5)$$

and this equation is used for computer solution of the age. Examples of well-expressed linear-trend plots are shown in Fig. 2.

An additional parameter, taken from the slope graphics of the plot, is the intercept, x_i on the X-axis, of the line represented by

$$y = mx + b \quad (6)$$

$$x_i = -b/m \quad (7)$$

where m is the measured slope of the line, b is the intercept on the Y-axis, and x_i is the intercept on the X-axis. The value of x_i is used to obtain time calibration for the uranium-trend model (discussed below).

A different plot of the isotopic data can be constructed when the $^{238}U/^{232}Th$ ratios of the samples are plotted on the X-axis versus the $^{230}Th/^{232}Th$ ratios plotted on the Y-axis. This thorium-index plot is used to determine whether all the samples included in the uranium-trend line describe a reasonably linear array with respect to thorium. Samples representing different depositional units commonly have different initial U/Th ratios; therefore, this plot sometimes serves as a useful check to determine if all samples are from the same depositional unit.

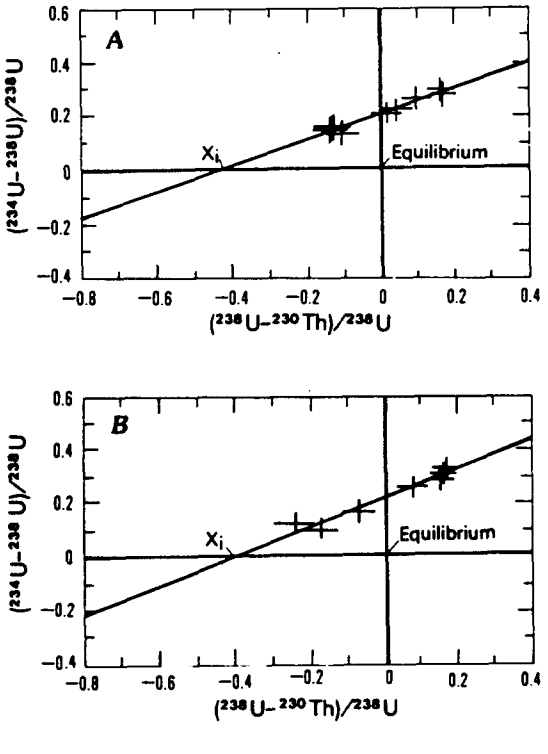

FIG. 2. Examples of uranium-trend plots that show good linearity and yield U-trend ages that are in agreement with independent age control. Example is from Fig. 11.3 of Rosholt *et al.* (1988).

Calibration

The value λ_0 is the decay constant for F(0). It is strictly an empirical value that allowed selection of the proper coefficients (C_1, C_2, C_3, C_4, C_5) for the exponential terms in Eq. 4. For deposits of unknown age, a method is required to determine the proper λ_0 value to be used in Eq. 4; this is done with a calibration curve that is based on values of λ_0 determined for deposits of known age. For deposits of known age, the quantity x_i (Eq. 7) is plotted against the half period of F(0) on a log–log plot as shown in Fig. 3. The calibration curve was determined by selecting the proper λ_0 value that yielded the correct age for independently-dated calibration deposits using the model equation. The x_i values of known-age deposits are used for calibration (Fig. 3) and these values are plotted against the half periods of F(0) equivalent to their λ_0 values; half periods are plotted instead of λ_0's because of their numerical convenience. For deposits whose analyses are included in this report, F(0) is determined from Fig. 3 using the x_i value measured on the uranium-trend plot of the data for each depositional unit. The decay pattern for deposits in different environments varies with different F(0) values.

Four primary calibration points based on different radiometric dating techniques were used to develop the calibration curve in Fig. 3. These calibration points include: (1) the radiocarbon ages of about 12 ka for Peoria loess in Minnesota (Frye, 1973); (2) the obsidian hydration age (calibrated by K–Ar ages) of 150 ± 15 ka (Rosholt, 1985), for glacial deposits of Bull Lake age in southwestern Montana and northwestern Wyoming (Pierce, 1979); (3) the K–Ar age of 0.61 ± 0.01 Ma for the Lava Creek B ash for the age of the zeolitized ash in Tuff A at Lake Tecopa, California (J. D. Obradovich, *pers. commun.*, 1987); and (4) the K–Ar age of 0.74 ± 0.01 Ma for the Bishop ash for the age of Tuff B at Lake Tecopa (Hurford and Hammerschmidt, 1985). In

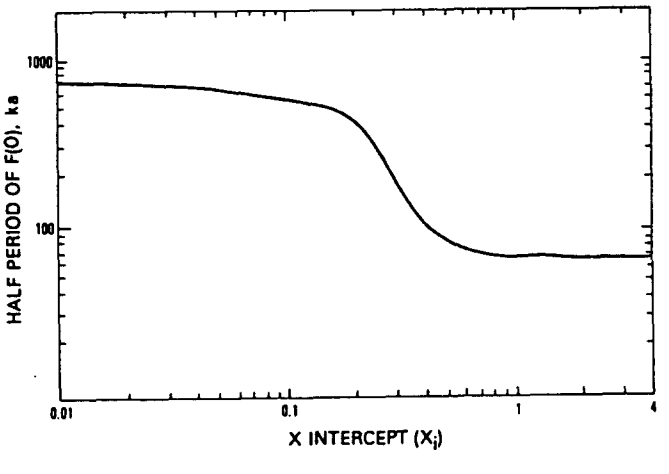

FIG. 3. Time-calibration curve for determination of uranium flux F(0), from x-intercept value (Rosholt, 1985).

addition, a number of other radiometric ages were also used as secondary calibration points (Rosholt *et al.*, 1985a).

PROBLEMS AND LIMITATIONS

Because uranium-trend dating is applied to bulk samples of sediment or soil material, the measured isotopic abundances reflect the influence of a complex assemblage of mineral and organic components. The numerous geochemical variables which preclude the development of a rigorous mathematical model to describe the isotopic evolution of such a system also make U-trend dating of some deposits unfeasible. We have already mentioned that one of the prerequisites for successful application of the U-trend dating method is sufficient mixing of sediment during transport and deposition such that $^{234}U/^{238}U$ ratios of recently deposited sediments are similar with depth. In addition, we have identified a number of geochemical and geologic conditions that can develop subsequent to deposition that can sometimes make application of the U-trend method unfeasible. These conditions are based on observations made in previous studies (Rosholt, 1985; Rosholt *et al.*, 1966, 1985a, b). They can usually be easily identified after U-trend analyses are completed because they are indicated by data points that depart significantly from linearity on either the U-trend or thorium-index plots. Examples of well-defined U-trend plots are shown in Figs 1A and 1B. Figure 4 illustrates a variety of non-linear plots that result from the following conditions:

(1) Mechanical mixing of deposits of different age (Fig. 4a). Mixing after deposition can result from physical and/or biotic processes.

(2) Fixed-phase (solids dominant) U concentrations that are significantly greater than mobile-phase (water dominant) U concentrations (Figs 4b, c).

(3) Recent interaction of the deposit with waters of high U concentration after a long period of interaction with waters of low U concentration (Fig. 4d).

(4) Deposits to be dated are deeply buried by younger deposits of low permeability; thus, the older deposits are likely to experience little or no interaction with migrating U-bearing water (Figs 4b, c).

(5) Deposit or soil material behaves more like a closed than an open system because of geochemical or pedogenic precipitates, such as secondary calcium carbonate (Fig. 4e).

(6) Deposits have a low surface area/mass ratio and thus have little adsorptive capacity for ^{238}U daughter products, as is the case with well-sorted sand (Fig. 4b).

(7) Deposit has uniform mineralogy resulting in similar U–Th isotopic abundances throughout the deposit (Fig. 4b).

(8) Actual age of deposit is less than 5 ka (Figs 4b or c) or greater than 700 ka (Fig. 4f).

In addition, a complex geologic history can result in an inaccurate U-trend age even when a U-trend plot shows reasonable linearity. For example, the lower part

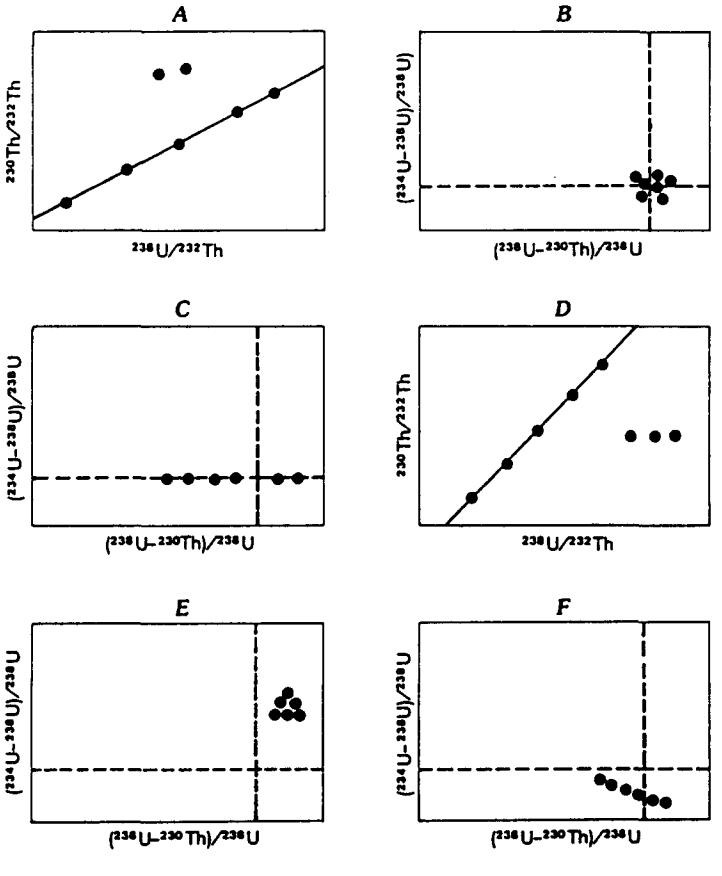

FIG. 4. Hypothetical arrays of points on U-trend and Th-index plot that show conditions making U-trend dating unfeasible (see text for discussion). Dashed lines mark equilibrium values on U-trend plots.

of a deposit to be dated might experience little or no interaction with U-bearing water (as described above) during its history. At some later time, however, the upper part of the deposit is removed by erosion and the lower part begins to experience interaction with U-bearing water. The U-trend age will reflect the time of sediment/water interaction, not the original time of sediment deposition. This is a condition that can be assessed only by geologic evidence and/or independent age control, because the deposit may yield well-defined Th-index and U-trend plots. If independent age control exists, the apparent U-trend age may indicate the time of exhumation of the deposit.

Unless the physical, chemical, and mineralogical properties of a deposit or soil to be dated are adequately characterized, it is often not possible to predict, in advance, if some of the above conditions apply, particularly conditions 1, 2, 3, 7, and 8. Thus, in most cases, the main criterion for assessing the suitability of a deposit or soil material for U-trend dating is the deposit's U-trend plot or its Th-index plot. Because of the potentially unfavorable conditions that may exist, great care needs to be taken in evaluating and sampling the deposit before laboratory analyses are undertaken.

In summary, we suggest the following guidelines for evaluating the reliability of a calculated U-trend age:

(1) The U-trend plot should show good linearity.

(2) The U-trend plot should show reasonable 'extension', i.e., a sufficient range, greater than 10% of sample isotopic variation, that is indicative of genuine isotopic variability in the analyzed deposit or soil material.

(3) The Th-index plot should show good linearity.

(4) The calculated U-trend age should be consistent with the deposit's stratigraphic relationships and any independent age determinations.

Limitations for the precision of the U-trend dating method result from analytical procedures. A brief description of these procedures is as follows, and readers are referred to Rosholt (1984, 1985) for details. The bulk sediment or soil samples are passed through a 2 mm sieve and the less-than-2 mm fraction is decomposed with a mixture of concentrated HF, HNO_3 and $HClO_4$ after the addition of a combined spike of ^{236}U and ^{229}Th. The residue is dissolved in HCl and U and Th are separated by ion exchange methods. Further purification of U and Th is done by a combination of solvent-extraction, ion-exchange and coprecipitation methods. The purified U and Th separates are plated on platinum or stainless steel discs (Rosholt, 1985). Uranium and thorium separates are measured individually in high-resolution alpha spectrometers and a large-capacity multichannel analyzer with multiple input capability. Partially depleted silicon surface barrier detectors are used in the spectrometers. Normally, a minimum of 10,000 counts in the integrated portion of each alpha-energy peak is accumulated for each measurement. For defining linear trends, good counting statistics are required and a uranium sample is usually counted (to 10,000 counts each) in four different detectors and the resultant values are averaged. A thorium sample is usually counted three separate times and the resultant values are averaged. Because of the specific spikes used, the alpha peaks do not require correction for ingrowth of daughter products. It was not necessary to correct the alpha peaks for background contribution because of the relatively high count rates obtained. The $^{238}U/^{236}U$ activity ratio is used to determine the uranium concentration by radioisotope dilution using a ^{236}U spike calibrated with a standard uraninite solution (Rosholt, 1984). The $^{232}Th/^{229}Th$ activity ratio is used to determine thorium concentration. The $^{230}Th/^{229}Th$ activity ratio is used to determine ^{230}Th content by radioisotope dilution with a ^{229}Th spike calibrated with a standard Harwell uraninite solution (Ivanovich *et al.*, 1984). The concentrations of ^{238}U and ^{230}Th in the standard uraninite solution are calibrated with NBS 950 standard uranium. Activity ratios of $^{234}U/^{238}U$ and $^{230}Th/^{232}Th$ are measured directly from the spectra; activity ratios of $^{230}Th/^{238}U$ and $^{238}U/^{232}Th$ and activity ratios used for U-trend plots are calculated from data obtained in both the U and Th spectra where

$$\frac{^{230}Th}{^{238}U} = \frac{\mu g \text{ equiv. } ^{230}Th}{\mu g\ ^{238}U} \tag{6}$$

$$\frac{^{238}U}{^{232}Th} = \frac{^{230}Th/^{232}Th}{^{230}Th/^{238}U}. \tag{7}$$

Uranium isotopic ratios determined by four separate measurements (10,000 counts each), each counted with a different detector, indicate that the standard deviations in each of the isotopic ratios exceed the value of the errors calculated from counting statistics. Therefore, the standard deviation of the four measurements is used to obtain a 2σ error value. The same procedure is used to obtain the 2σ error value for thorium isotopic ratios that are based on three separate 10,000 count runs. The computer program used to calculate the slope and uncertainties in the slope of the linear trend specifies that 2σ error values should be used to obtain a fit of the line to the measured data (York, 1969). Typically, 2σ values of 2.8% for $^{230}Th/^{232}Th$, 5.2% for $^{238}U/^{232}Th$, 3.2% for $^{234}U/^{238}U$, and 4.2% for $^{230}Th/^{238}U$, were determined from standard deviations for several measurements on a variety of samples.

Linear Trend Plots and Linear Regression Calculations

A computer program is used to generate Cartesian plots of both the uranium-trend data and the thorium-index data. The program, modified from that of Ludwig (1979), is also used to calculate best-fit linear trends. After the data are plotted, a least squares regression line is calculated using a modified York (1969) fit, which assumes that both X and Y parameters have associated errors and that all deviation from a straight line is due to normally distributed analytical error. As discussed above, the program requires that 2σ analytical errors are included with each isotopic ratio.

The resulting error in the calculated straight line is 1σ including the observed scatter. The uncertainty in the regression line is asymmetric except at low values. To correct for this asymmetry, the uncertainty of the angle, θ, of the regression line with the X-axis is also calculated, so that the errors on the slope of the regression line are angularly symmetric with respect to the best-fit line. Equations for determining the angular uncertainty are given by Ludwig (1980).

CASE STUDIES OF SOUTHERN CALIFORNIA MARINE TERRACES

Palos Verdes Hills

The Palos Verdes Hills area near Los Angeles is a crustal block bounded on its northeastern flank by the northwest-trending Palos Verdes fault. Woodring *et al.* (1946) mapped 13 marine terraces which are mostly cut on shales of the Miocene Monterey Formation (Fig. 5). Marine terrace deposits are usually 1–3 m thick and are often overlain by non-marine alluvial or colluvial deposits which vary greatly in thickness.

We sampled marine terrace deposits from the 1st, 4th and 12th terraces for uranium-trend dating (Table 1 and Fig. 5). At all sites, thin non-marine deposits overlie the marine sediments. The marine sediments consist of calcareous, fossiliferous, poorly-sorted sands and gravels, largely derived from the Monterey Formation. Calcium carbonate content of the less-than-2 mm fraction of these sediments is high, ranging from 54–86% (Table 2). The carbonates in these sediments are derived partly from the Monterey Formation and partly from weathering of marine fossils. Uranium content ranges from 1.9–9.7 ppm, and shows no obvious relationship to $CaCO_3$ content (Table 2).

The ages of the 1st terrace in the San Pedro area (where PVH1 was sampled) and the 2nd terrace in the Palos Verdes Hills area are thought to be 80–120 ka based on aminostratigraphic correlation (Muhs and Rosholt, 1984). We estimated ages for the 4th and 12th terraces using their shoreline angle elevations, an assumption of sea levels close to the present at the time of terrace formation, and an assumption of a constant uplift rate. An uplift rate of 0.33 m/ka is calculated using the shoreline angle elevation of 46 m for terrace 2, its estimated age of 120 ka, and an assumption that sea-level was about +6 m relative to present at 120 ka (Ku *et al.*, 1974). By this method, the 4th and 12th terraces are estimated to be ~275 ka and ~1130 ka, respectively.

Both Th-index and U-trend plots for PVH1 and PVH4 are highly linear with correlation coefficients greater than 0.96 for all of the plots (Figs 6 and 7 and Table 3), although we note that PVH4 shows little 'extension' or isotopic variability. The calculated U-trend ages for PVH1 and PVH4 are 150 ± 50 and 230 ± 60 ka, respectively, and are consistent with their estimated ages (Table 1). We

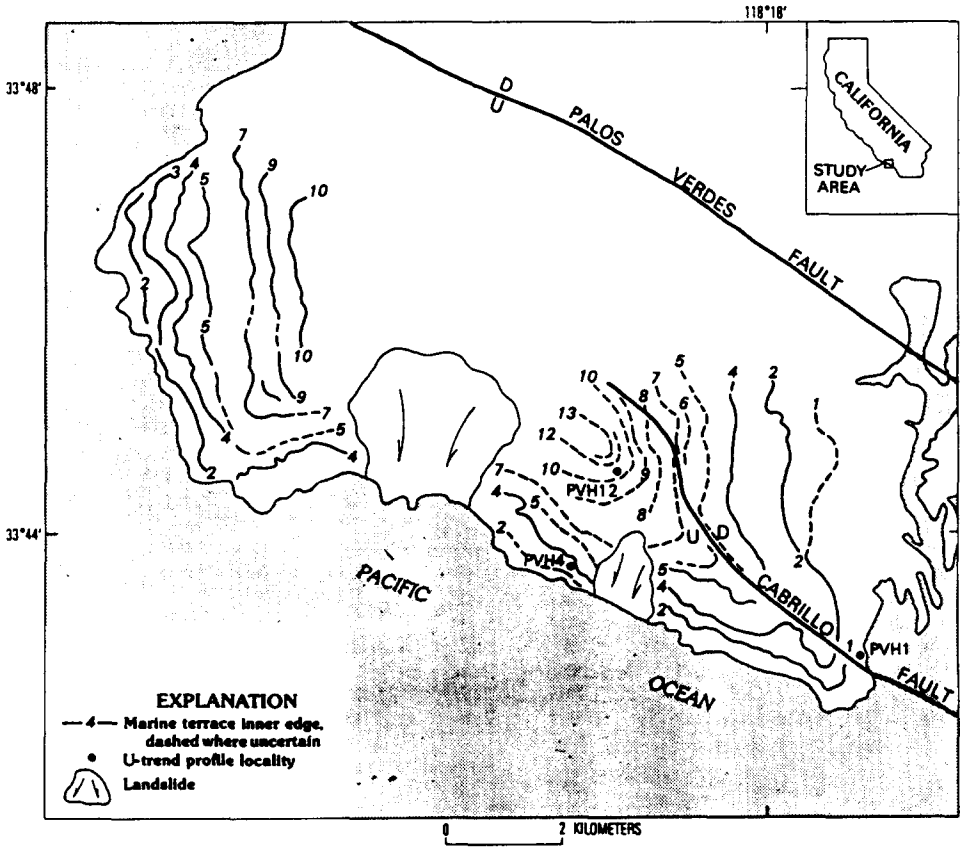

FIG. 5. Map showing marine terrace inner edges, landslides, major faults, and U-trend sample localities in the western part of the Palos Verdes Hills. Marine terrace inner edges are from Woodring *et al.* (1946).

TABLE 1. Locations, terrace numbers, elevations of shoreline angles, amino acid ratios in fossil *Tegula* and independent age estimates of marine terrace deposits sampled for U-trend dating

Profile no.	Location	Terrace	Elevation (m)	Mean Alle/Ile	Age (ka)	Method of age determination	Reference
PVH1	Palos Verdes Hills	1	40	0.55 ± .06[a]	~80–120	Aminostratigraphic correlation	Muhs and Rosholt (1984)
PVH4	Palos Verdes Hills	4	91	0.62 ± .08	275	Uplift rate estimate	This study
PVH12	Palos Verdes Hills	12	373	1.00 ± .10	1130	Uplift rate estimate	This study
SNI1	San Nicolas Island	1	11	0.29 ± .05	80 ± 4	$^{230}Th/^{234}U$, corals	Muhs *et al.* (1987)
SNI2	San Nicolas Island	2	33	0.43 ± .05	115 ± 8 122 ± 8	$^{230}Th/^{234}U$, corals	Muhs *et al.* (1987)
SNI2A	San Nicolas Island	2	33	0.43 ± .05	115 ± 8 122 ± 8	$^{230}Th/^{234}U$, corals	Muhs *et al.* (1987)
SNI4	San Nicolas Island	4	97	1.04 ± .07	440	Uplift rate estimate	This study
SNI5	San Nicolas Island	5	118	1.07 ± .06	535	Uplift rate estimate	This study
SNI8	San Nicolas Island	8	183	1.24 ± .04	830	Uplift rate estimate	This study
SNI10	San Nicolas Island	10	238	1.25 ± .03	1080	Uplift rate estimate	This study

[a] Mean Alle/Ile ratio in *Tegula* given is for a terrace mapped as terrace 2 by Woodring *et al.* (1946). Terrace 2 may be correlative with what Woodring *et al.* (1946) mapped as terrace 1 in the Cabrillo Beach area, where PVH1 is located (see Muhs and Rosholt, 1984).

TABLE 2. Estimated $CaCO_3$ contents, uranium and thorium concentrations, Th/U ratios, and isotopic activity ratios of marine terrace sediments

Profile no.	Depth below surface (cm)	$CaCO_3$[a] (%)	U (ppm)	Th (ppm)	Th/U	$^{234}U/^{238}U$	$^{230}Th/^{238}U$	$^{238}U/^{232}Th$	$^{230}Th/^{232}Th$
PVH1	6–12	70.0	3.77	3.06	0.81	0.963	0.959	6.239	5.980
	12–26	68.4	3.37	2.66	0.79	0.947	1.033	3.860	3.989
	30–38	60.7	4.10	2.00	0.49	0.942	1.056	3.756	3.966
	40–50	66.6	4.52	2.01	0.44	0.964	0.936	6.881	6.441
	50–56	70.0	5.29	2.21	0.42	0.978	0.905	7.308	6.614
PVH4	216–239	82.3	2.11	1.03	0.49	0.958	1.053	6.386	6.724
	239–262	52.0	2.26	3.10	1.37	0.885	1.261	2.234	2.801
	262–282	64.8	2.03	2.22	1.11	0.896	1.254	2.782	3.488
	282–302	67.5	1.89	2.34	1.24	0.913	1.223	2.468	3.018
	302–325	56.6	1.79	3.14	1.76	0.894	1.288	1.790	2.306
	325–356	47.5	1.90	3.81	2.01	0.901	1.257	1.519	1.909
PVH12	112–142	80.6	2.43	0.61	0.25	1.065	1.202	12.26	14.73
	152–182	77.9	2.06	0.61	0.30	1.040	1.132	10.42	11.80
	182–213	54.7	9.67	2.54	0.26	1.073	1.142	11.59	13.24
	214–244	86.6	4.10	1.08	0.26	1.084	1.276	11.67	14.89
	245–275	85.4	2.25	0.87	0.39	1.019	1.120	7.93	8.88
SNI1	690–700	87.4	1.54	1.71	1.10	1.409	0.892	2.796	2.496
	700–710	83.4	1.71	2.03	1.18	1.415	0.930	2.610	2.428
	710–720	70.6	1.68	2.73	1.62	1.330	0.919	1.902	1.747
	720–730	61.0	1.93	4.40	2.28	1.224	0.909	1.356	1.233
	730–740	61.3	1.53	2.87	1.87	1.263	0.929	1.649	1.532
	740–750	59.6	1.33	2.98	2.24	1.266	0.939	1.379	1.296
	750–760	44.5	1.25	3.99	3.19	1.158	0.977	0.970	0.947
	760–770	67.8	1.32	3.39	2.55	1.223	1.041	1.210	1.260
SNI2	0–10	73.7	1.32	3.22	2.45	1.144	1.022	1.263	1.290
	10–20	63.6	1.16	2.65	2.28	1.151	0.960	1.358	1.303
	20–30	63.4	1.26	2.69	2.13	1.176	0.954	1.450	1.383
	30–40	54.4	1.26	3.00	2.38	1.205	0.997	1.297	1.293
	40–50	61.0	1.15	2.42	2.11	1.295	1.012	1.464	1.483
	50–57	60.9	1.30	2.67	2.05	1.275	1.053	1.509	1.589

Continued over

TABLE 2 (*continued*)

Profile no.	Depth below surface (cm)	$CaCO_3$[a] (%)	U (ppm)	Th (ppm)	Th/U	$^{234}U/^{238}U$	$^{230}Th/^{238}U$	$^{238}U/^{232}Th$	$^{230}Th/^{232}Th$
SNI2A	0–15	27.5	2.18	8.87	4.06	1.034	0.964	0.761	0.733
	15–30	26.1	2.30	10.77	4.69	1.002	1.039	0.659	0.684
	30–45	39.1	1.79	6.96	3.88	1.034	0.957	0.796	0.762
	45–60	32.8	1.71	6.90	4.02	1.048	1.088	0.768	0.835
	60–75	40.4	1.73	6.67	3.85	1.016	1.018	0.803	0.817
	75–90	49.0	1.44	4.70	3.26	1.020	0.973	0.946	0.921
	90–105	49.6	1.49	5.17	3.46	1.028	1.013	0.893	0.904
	105–120	67.6	1.13	2.94	2.60	1.079	0.968	1.188	1.150
	120–135	84.2	1.16	1.17	1.01	1.114	0.709	3.044	2.159
SNI4	230–240	59.5	1.39	2.90	2.09	1.269	1.327	1.480	1.964
	240–250	72.2	1.46	2.19	1.50	1.323	1.371	2.060	2.824
	250–260	61.6	1.67	2.76	1.65	1.342	1.348	1.867	2.517
	260–270	53.7	1.56	3.89	2.49	1.260	1.209	1.239	1.498
	270–280	74.0	1.64	3.36	2.04	1.257	1.244	1.511	1.880
	280–290	71.3	1.38	2.77	2.01	1.486	1.754	1.539	2.699
	290–300	62.2	1.46	3.61	2.47	1.403	1.594	1.252	1.995
	300–310	63.7	1.32	3.59	2.71	1.436	1.715	1.140	1.956
SNI5	10–20	71.4	0.61	1.45	2.38	1.107	1.187	1.298	1.541
	20–30	79.8	0.54	0.92	1.71	1.161	1.108	1.806	2.001
	30–40	82.1	0.67	1.37	2.05	1.142	1.285	1.510	1.940
	40–50	91.5	0.62	0.83	1.33	1.195	1.255	2.323	2.916
	50–60	88.9	0.81	1.39	1.71	1.158	1.109	1.803	1.999
	70–80	57.8	1.21	4.46	3.70	1.062	1.044	0.836	0.874
	80–90	47.1	1.30	5.14	3.95	1.021	1.028	0.783	0.805
	90–100	34.8	1.85	7.63	4.12	0.984	0.997	0.750	0.748
SNI8	210–220	73.9	1.25	6.87	5.50	1.064	1.221	0.562	0.686
	220–230	42.1	1.40	9.94	7.09	0.961	1.138	0.436	0.496
	230–240	58.9	1.22	8.86	7.29	1.065	1.325	0.424	0.562
	240–250	46.3	1.34	9.34	6.97	1.027	1.236	0.443	0.548
	250–260	70.7	2.11	5.74	2.72	1.016	0.994	1.134	1.128
	260–270	55.9	1.53	8.68	5.71	1.029	1.194	0.544	0.649
	270–280	52.3	1.48	7.65	5.16	1.008	1.114	0.599	0.667
	280–290	50.9	1.49	8.70	5.82	1.076	1.256	0.531	0.667
SNI10	0–10	63.9	0.92	1.52	1.66	1.073	1.136	1.862	2.115
	10–20	72.5	1.03	1.84	1.79	1.000	1.103	1.726	1.903
	20–30	78.2	0.91	1.92	2.11	1.070	1.159	1.468	1.701
	30–40	74.0	1.12	2.77	2.49	1.034	1.056	1.242	1.312
	40–50	89.6	0.91	1.35	1.49	1.100	1.242	2.078	2.579
	50–60	91.4	0.84	0.86	1.02	1.129	1.207	3.042	3.673
	60–70	92.2	0.80	0.76	0.94	1.154	1.248	3.281	4.096

[a] Estimated from weight loss on ignition at 900°C for eight hours for material less than 2 mm in size; $CaCO_3$ contents reported are probably maximum values.

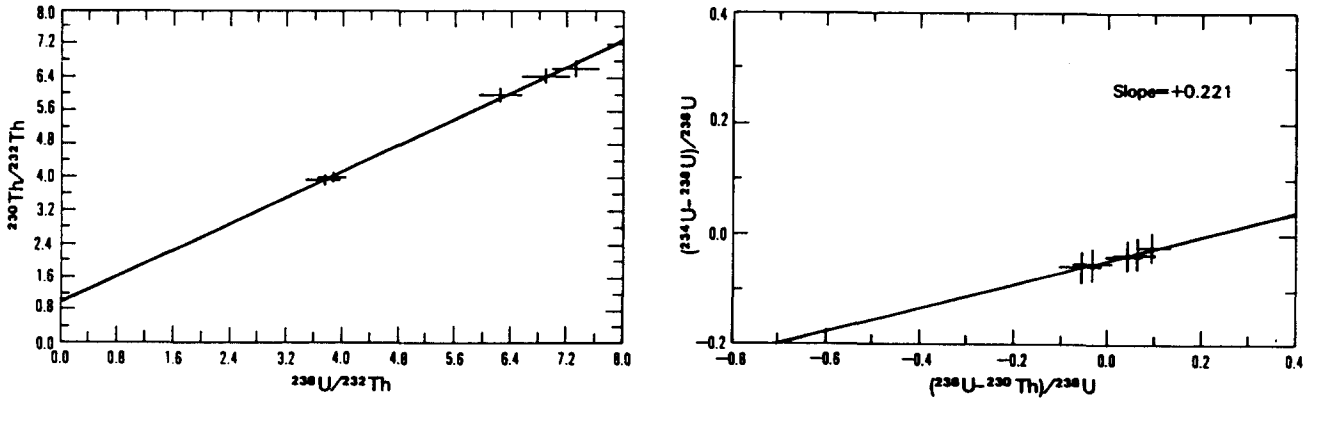

FIG. 6. U-trend and Th-index plot for PVH1.

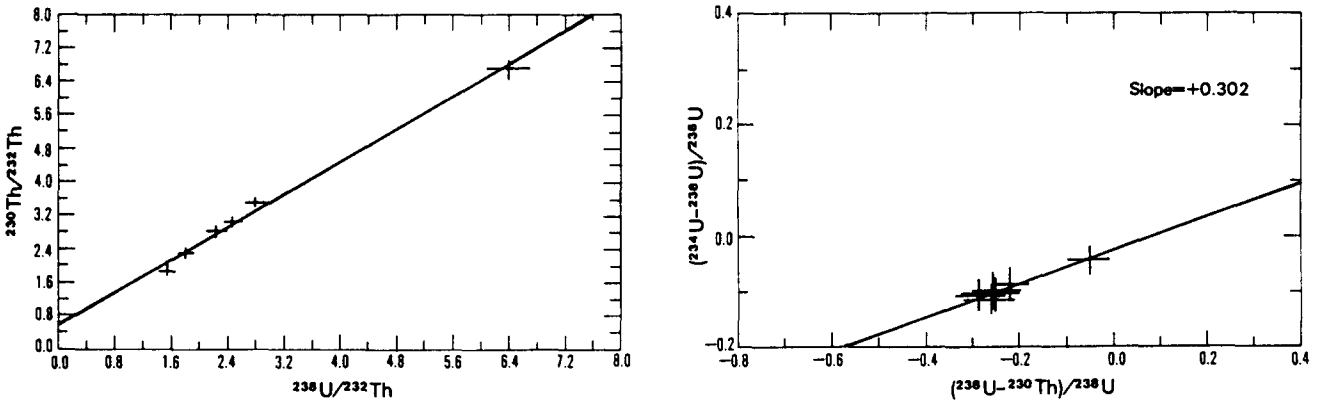

FIG. 7. U-trend and Th-index plot for PVH4.

TABLE 3. Correlation coefficients of Th-index plots and U-trend plots, U-trend parameters, and U-trend ages

Profile no.	Th-index plot correlation coefficient	Confidence level (%)	U-trend plot correlation coefficient	Confidence level (%)	U-trend slope	U-trend slope error	*X*-intercept	Half-period of F(0) (ka)	Age[a] (ka)
PVH1	0.998	99.9	+0.984	99.8	+0.221	0.015	+0.209	408	150 ± 50
PVH4	0.998	99.9	+0.969	99.9	+0.302	0.026	+0.082	596	230 ± 60
PVH12	0.971	99.4	−0.764	86.7	−0.360	0.103	+0.019	698	>700
SNI1	0.996	99.9	+0.565	85.5	+1.101	0.657	+0.202	419	nd
SNI2	0.899	98.5	−0.580	77.3	−0.978	0.686	+0.212	402	nd
SNI2A	0.994	99.9	+0.766	98.4	+0.326	0.058	+0.098	578	240 ± 30
SNI4	0.792	98.1	−0.973	99.9	−0.404	0.028	+0.413	104	390 ± 50
SNI5	0.989	99.9	−0.775	97.6	−0.702	0.130	+0.021	689	550 ± 80
SNI8	0.988	99.9	−0.623	90.1	−0.232	0.119	+0.052	644	>700
SNI10	0.997	99.9	−0.859	98.7	−0.735	0.117	+0.056	637	530 ± 60

[a] nd — not determined.

are less certain about the estimated age of >700 ka for the 12th terrace, PVH12. Although the Th-index plot shows good linearity (Fig. 8), the U-trend plot has a correlation coefficient of only −0.764, which is significant only at a confidence level of ~87% (Table 3). Despite this uncertainty, the U-trend age estimate of >700 ka does not conflict with the uplift rate age estimate of 1130 ka, and is significantly older than the U-trend age estimate of the 4th terrace. The U-trend age for PVH12 is also supported by amino acid ratios, which are significantly higher in molluscs from the 12th terrace than in molluscs from the 4th terrace (Muhs and Rosholt, 1984). Because the U-trend plots show generally good linearity and calculated ages for the three terraces are in correct stratigraphic order, we conclude that U-trend dating of poorly-sorted, calcareous terrace sediments derived from rocks such as the Monterey Formation is feasible.

San Nicolas Island

San Nicolas Island is a crustal block composed primarily of Eocene siltstones and sandstones overlain by Quaternary marine terrace deposits, dune sand, and eolianite. Structurally, this island is a complexly faulted anticline; a major, northwest-trending offshore fault parallels the southern coast of the island (Vedder *et al.*, 1974). Vedder

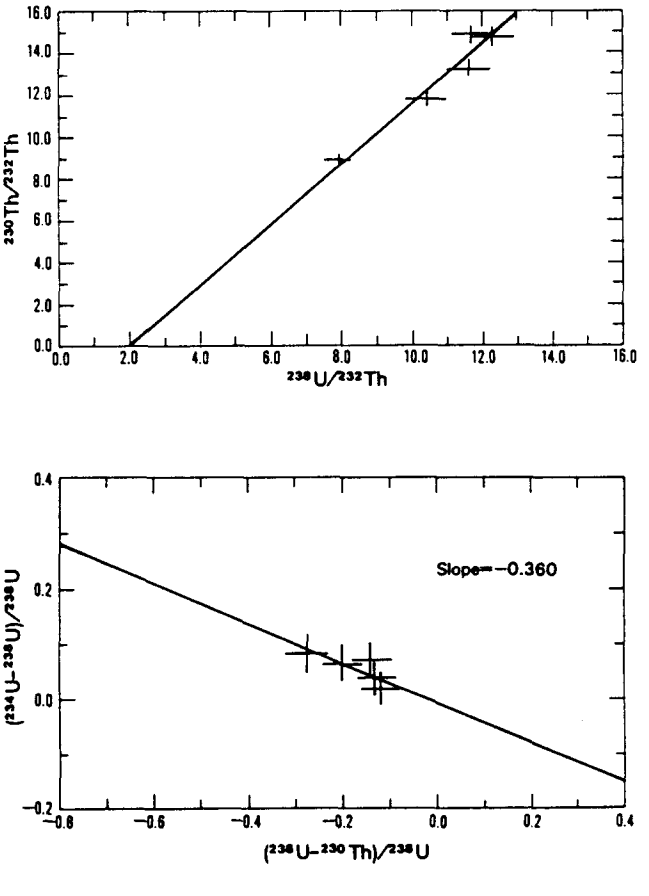

FIG. 8. U-trend and Th-index plot for PVH12.

and Norris (1963) mapped 14 marine terraces on San Nicolas Island which rise to a maximum elevation of ~277 m (Fig. 9). The terraces are not as well expressed geomorphically as they are on the Palos Verdes Hills, owing to a cover of non-marine deposits such as eolianite, dune sand, or alluvium that in some places may be as much as 15 m thick. This cover is significant for sampling strategies of U-trend dating studies for reasons discussed earlier. Care was taken to sample only marine terrace deposits that were either exposed at the surface or have experienced only shallow burial by non-marine deposits. Most marine terrace deposits on San Nicolas Island are highly calcareous; they range from 26–92% $CaCO_3$ and average about 65% $CaCO_3$ (Table 2). The carbonates are derived from Quaternary fossil molluscs, echinoids, corals, algae, and bryozoans. The non-carbonate fraction consists of gravels and sands derived from the Eocene siltstones and sandstones, plus an unknown amount of infiltered eolian silt and clay derived from distant sources (Muhs, 1983b). Uranium content is fairly low in all terrace deposits studied, ranging from 0.6–2.3 ppm, and shows an inverse relationship with $CaCO_3$ content for SNI2A and SNI5, the two profiles with the greatest variability in $CaCO_3$ content (Table 2). For U-trend dating, we sampled deposits from the 1st, 2nd, 4th, 5th, 8th, and 10th terraces on San Nicolas Island. Two of these terrace deposits have U-series ages (on coral) in addition to their relative ages based on uplift rates (calculated from the age and elevation of the 2nd terrace) and amino acid ratios (Table 1).

In general, we obtained reasonable results for the older terraces but could not date the younger terraces. For the 1st and 2nd terraces (SNI1 and SNI2; Figs 10b and 11b), the U-trend plots indicate little variability on the $(^{238}U–^{230}Th)/^{238}U$ axes, with values that cluster near equilibrium, although the $(^{234}U–^{238}U)/^{238}U$ values show a typical range of variability. This poor linearity is reflected in low correlation coefficients (Table 3), and we have not attempted to calculate ages from these clustered plots. The lack of isotopic variability in profile SNI1 may be due to its relatively thick (~7 m) non-marine cover (Table 2); this is an example of condition 4 described earlier in the section on problems and limitations of U-trend dating. Deep burial cannot explain the clustering in SNI2, however. Because SNI2 also shows a clustering in the Th-index plot (Fig. 11a) and is only 57 cm thick, we resampled this deposit at another site on the 2nd terrace (SNI2A) landward of SNI2, where the terrace deposits are thicker and we hoped to find greater isotopic variability. The U-trend plot for SNI2A also shows little variability, with all but one point clustering around equilibrium values on both axes (Fig. 12b) although the plot has a marginally acceptable correlation coefficient (Table 3). However, the calculated age of 220 ± 30 ka is in disagreement with U-series ages of 115 ± 8 ka and 122 ± 8 ka on coral from this terrace reported by Muhs *et al.* (1987). We suspect there is insufficient mineralogic and/or chemical variability in the non-carbonate fraction of this profile to define a U-trend slope accurately. Results for the 4th terrace are much more reasonable than those for the lower two terraces (Fig. 13). The U-trend plot displays excellent linearity ($r = -0.962$) and extension, and the calculated age of 390 ± 45 ka is in

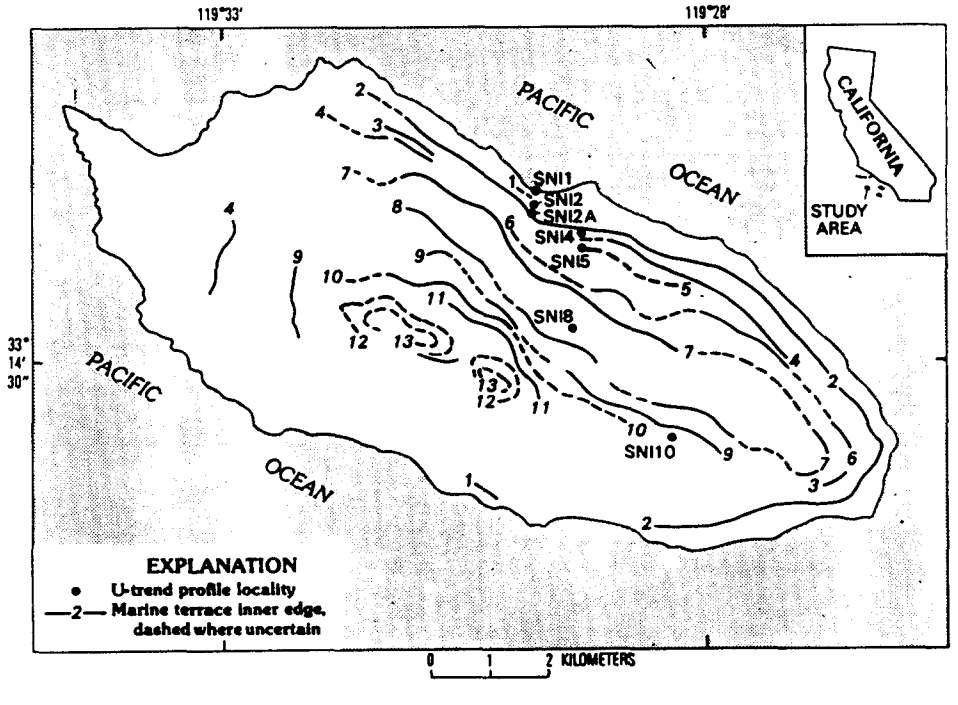

FIG. 9. Map showing marine terrace inner edges and U-trend sample localities on San Nicolas Island. Marine terrace inner edges are from Vedder and Norris (1963) and Muhs (1985).

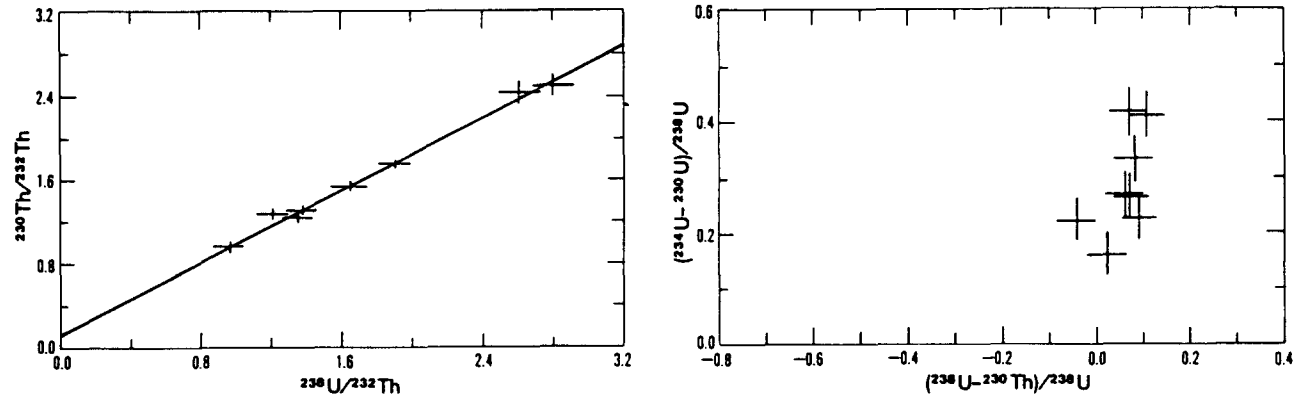

FIG. 10. U-trend and Th-index plot for SNI1. No U-trend slope is plotted because of the clustering of points.

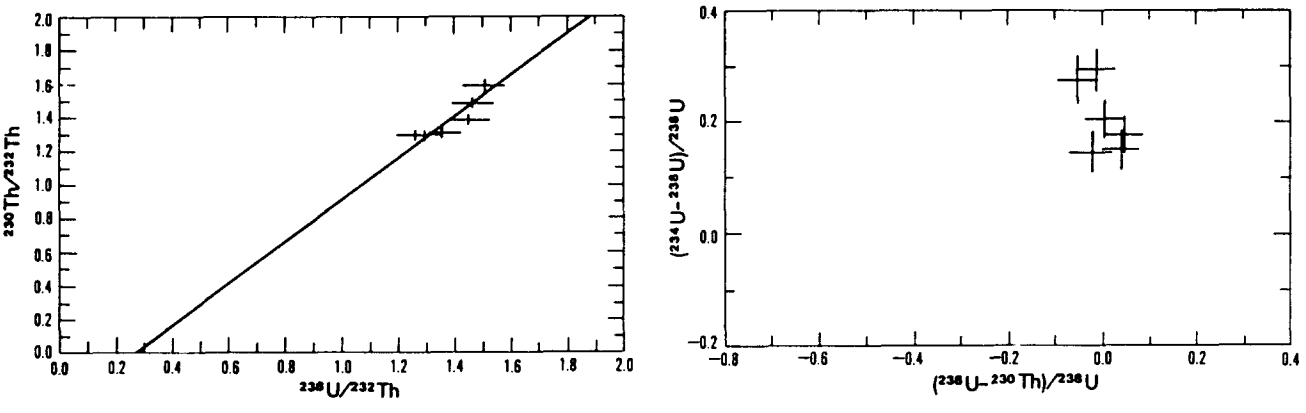

FIG. 11. U-trend and Th-index plot for SNI2. No U-trend slope is plotted because of the clustering of points.

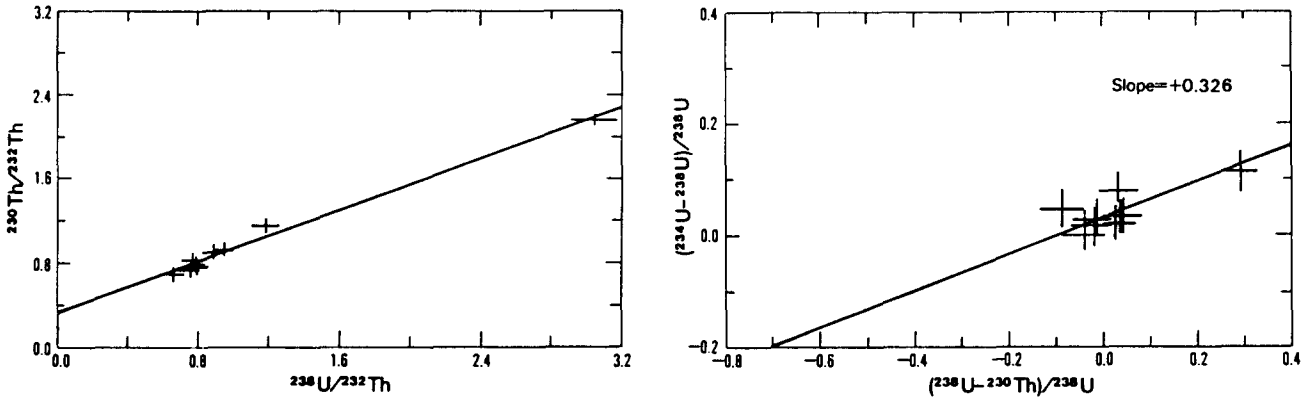

FIG. 12. U-trend and Th-index plot for SNI2A.

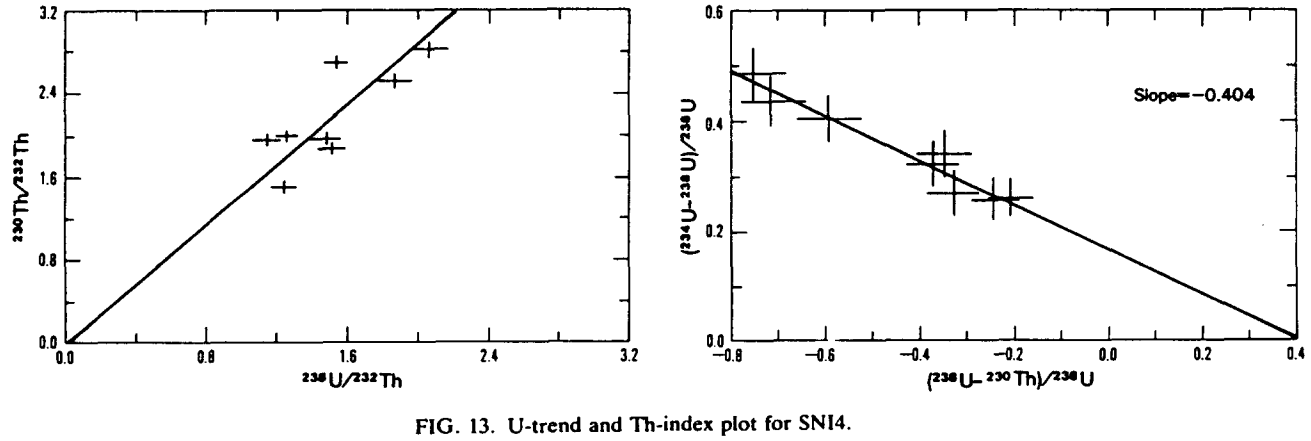

FIG. 13. U-trend and Th-index plot for SNI4.

reasonable agreement with the uplift rate age estimate of ~440 ka (Table 1). The Th-index plot of this deposit shows considerable scatter, however.

The three highest terraces studied, SNI5, SNI8 and SNI10, meet all of our criteria for acceptable U-trend ages. The Th-index plots for all profiles show excellent linearity and U-trend plots show fair to good linearity and extension (Figs 14, 15, 16). The age estimate of 550 ± 80 ka for SNI5 is in agreement with its uplift rate age estimate of ~535 ka (Table 1) and is significantly older than the U-trend age of SNI4. The age estimate of >700 ka for SNI8 does not conflict with the uplift rate age estimate of ~830 ka, and is significantly older than SNI4 and SNI5. However, the U-trend age of 530 ± 60 ka for SNI10 is neither consistent with its uplift rate age estimate nor amino acid ratios. The elevation of the 10th terrace is nearly twice that of the 5th terrace and amino acid ratios in *Tegula* from the 10th terrace are significantly greater than ratios in *Tegula* from the 5th terrace on San Nicolas Island and the 12th terrace on the Palos Verdes Hills (Table 1). U-trend results for SNI10 appear to represent an example of a condition described above in the section on problems and limitations. The marine terrace sediments at this locality are exposed at the ground surface with no soil cover (see Fig. 14 of Vedder and Norris, 1963) and fossils in the sediments are extremely well preserved, even to the extent of retention of original colors. Because we know of no other surface exposures of high-elevation terraces in California with such well-preserved fossils, we suggest that SNI10 once had a thicker, overlying sedimentary cover, and there was little sediment/water interaction until the present terrace sediments were exhumed after erosion of the overlying sediments. The U-trend age suggests that enough overlying material was removed for sediment/water interaction to begin by ~530 ka, or about the time of emergence of SNI5. SNI10 is an excellent example of a situation where a U-trend age must be carefully evaluated in terms of consistency with independent geologic evidence, because the age for this terrace cannot be rejected on the basis of the Th-index and U-trend plots. However, the results do suggest that U-trend dating may have the potential for unravelling subsequent erosional history of a deposit if reliable independent ages are available.

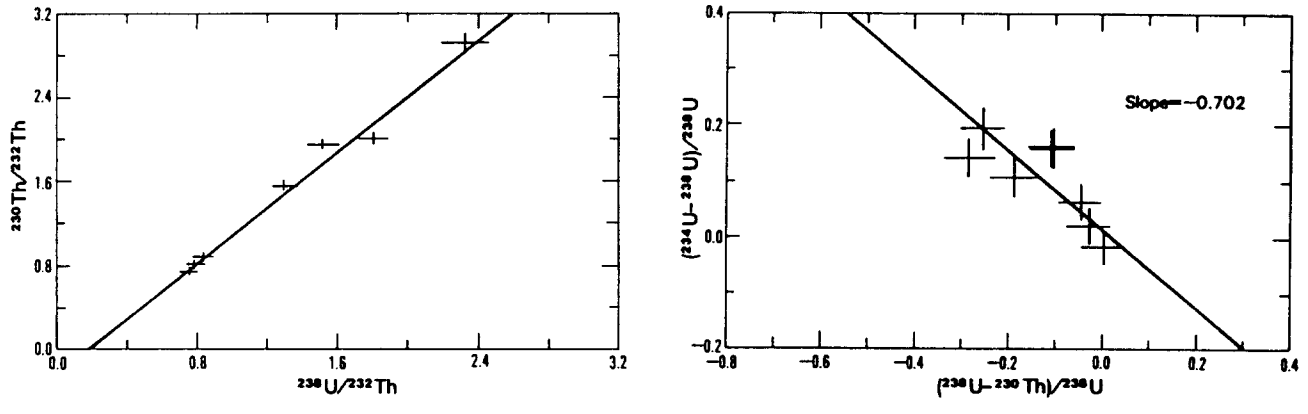

FIG. 14. U-trend and Th-index plot for SNI5.

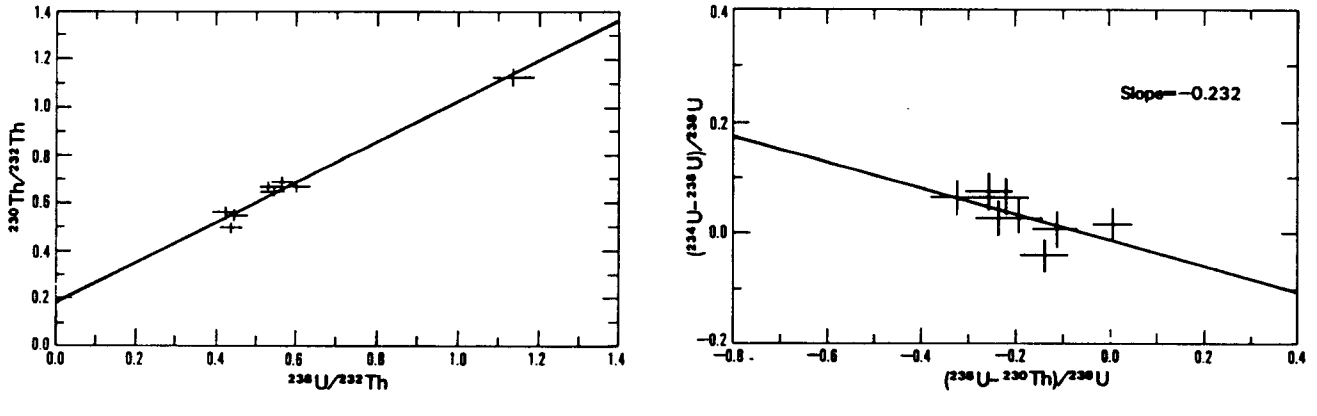

FIG. 15. U-trend and Th-index plot for SNI8.

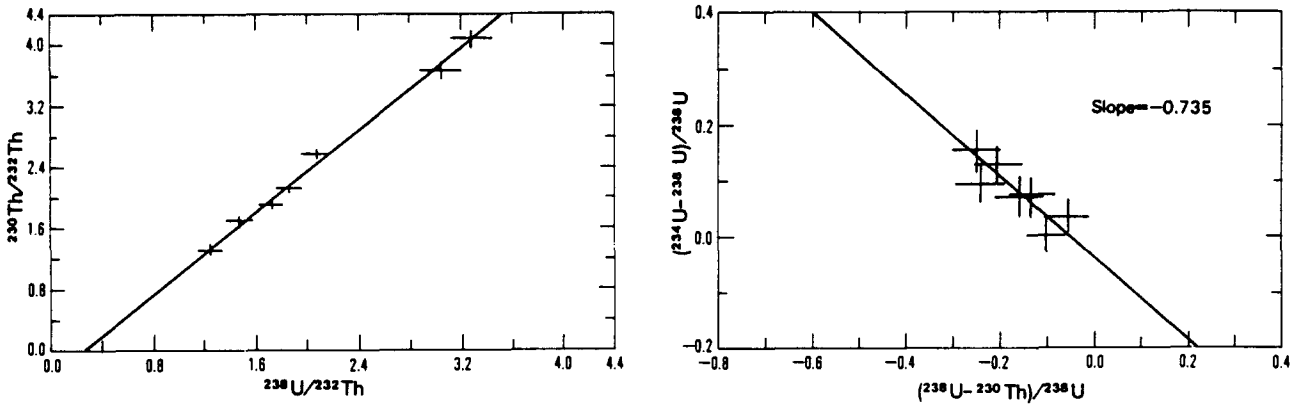

FIG. 16. U-trend and Th-index plot for SNI10.

Correlation of Marine Terraces with the Oxygen Isotope Record

Our U-trend age estimates for PVH1, PVH4, PVH12, SNI4, SNI5, and SNI8 show possible correlations with parts of the deep-sea marine oxygen isotope record of Shackleton and Opdyke (1973) (Fig. 17). We suggest that PVH1 and PVH4 are correlative with deep-sea isotope stages 5 and 7, respectively. SNI4 could correlate with either stage 11 or stage 13, and SNI5 most likely correlates with stage 15. On the basis of similar amino acid ratios, Muhs (1985) thought that SNI4 and SNI5 might represent individual sea-level highstands within a single oxygen isotope stage, or interglacial period. The U-trend age estimates, however, suggest that these two terraces probably represent separate interglacial periods (Fig. 17). Because the U-trend method only yields minimum ages for deposits older than 700 ka, we can only say that PVH12 and SNI8 are at least as old as deep-sea isotope stage 19. We suggest that U-trend dating has the potential for establishing correlations between middle Pleistocene marine terraces from many areas and the deep-sea oxygen isotope record.

CONCLUSIONS

We conclude that California marine terrace sediments can give reasonable U-trend ages provided that freshly deposited materials have sufficient mineralogic, textural, and chemical variability to yield a reasonable spread of points on U-trend and thorium-index plots. The youngest two terraces on San Nicolas Island are examples of geologic units that have very uniform isotopic compositions in the ^{238}U–^{234}U–^{230}Th system as a function of depth. Uniform isotopic composition is apparently not related to either $CaCO_3$ concentrations or U concentrations. More studies are needed to determine why these terraces yielded clustered U-trend plots. The oldest terrace on San Nicolas Island has a U-trend age much younger than is geologically reasonable, and suggests a complex erosional history. For other early-middle Pleistocene terraces on San Nicolas Island, and all terraces on the Palos Verdes Hills, U-

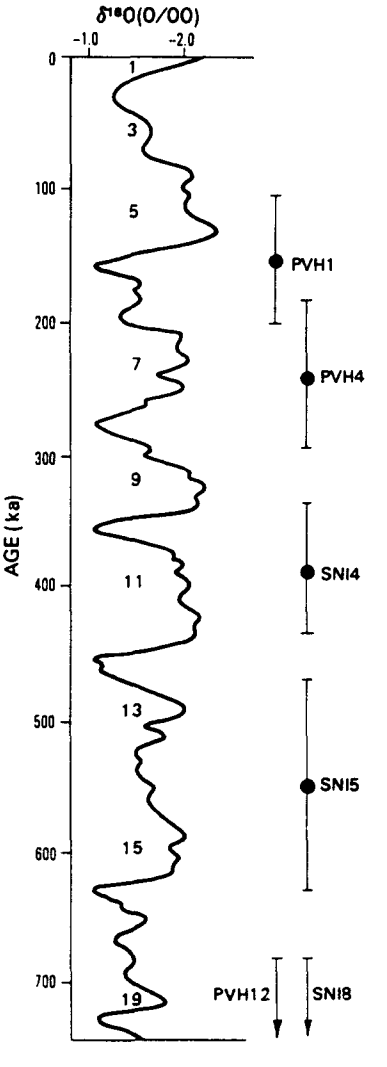

FIG. 17. Comparison of U-trend ages from the Palos Verdes Hills and San Nicolas Island with the oxygen isotope record in deep-sea core V28–238 from the equatorial Pacific. Oxygen isotope data from Shackleton and Opdyke (1973); timescale is derived from a sedimentation rate of 1.64 cm/ka, using an age estimate of 740 ka for the Brunhes–Matuyama boundary (Mankinen and Dalrymple, 1979) at 1200 cm. Numbers to left of curve are marine isotope stages.

trend ages are stratigraphically consistent and geologically reasonable. We suggest that U-trend dating of marine terrace sediments could yield important information in coastal tectonic studies, and new work should be initiated in other localities. For example, U-trend ages of high terraces along the Oregon coast could give long-term uplift rates for areas near the enigmatic Cascadia subduction zone (Heaton and Hartzell, 1987).

ACKNOWLEDGEMENTS

This study was conducted, in part, while Muhs held an NRC-USGS postdoctoral Research Associateship with Rosholt. Field work was supported in part by the Wisconsin Alumni Research Foundation. Tracy R. Rowland assisted in the field and Ron Dow of the U.S. Navy's Natural Resources Program provided logistical support for field work on San Nicolas Island. We thank the U.S. Navy for access to San Nicolas Island, and James E. Hadaway and Georgiann W. Rudder of the City of Los Angeles for access to localities in San Pedro and the Palos Verdes Hills. R. R. Shroba, B. J. Szabo, and an unknown reviewer read an earlier version of this manuscript and we thank them for their helpful comments.

REFERENCES

Ashby, J.R., Ku, T.L. and Minch, J.A. (1987). Uranium-series ages of corals from the upper Pleistocene Mulege terrace, Baja California Sur, Mexico. *Geology*, **15**, 139–141.

Birkeland, P.W. (1972). Late Quaternary eustatic sea-level changes along the Malibu coast, Los Angeles County, California. *Journal of Geology*, **80**, 432–448.

Bradley, W.C. and Griggs, G.B. (1976). Form, genesis, and deformation of central California wave-cut platforms. *Geological Society of America Bulletin*, **87**, 433–449.

Colman, S.M., Choquette, A.F., Rosholt, J.N., Miller, G.H. and Huntley, D.J. (1986). Dating the upper Cenozoic sediments in Fisher Valley, southeastern Utah. *Geological Society of America Bulletin*, **97**, 1422–1431.

Crittenden, R. and Muhs, D.R. (1986). Slope-angle and cliff-height relationships in a chronosequence of marine terraces, San Clemente Island, California. *Zeitschrift für Geomorphologie*, **31**, 291–301.

Frye, J.C. (1973). Pleistocene succession of the central interior United States. *Quaternary Research*, **3**, 275–283.

Hanks, T.C., Bucknam, R.C., Lajoie, K.R. and Wallace, R.E. (1984). Modification of wave-cut and faulting-controlled landforms. *Journal of Geophysical Research*, **89**, 5771–5790.

Harden, J.W., Sarna-Wojcicki, A.M. and Dembroff, G.R. (1986). Soils developed on coastal and fluvial terraces near Ventura, California. *U.S. Geological Survey Bulletin 1590-B*. 34 pp.

Heaton, T.H. and Hartzell, S.H. (1987). Earthquake hazards on the Cascadia subduction zone. *Science*, **236**, 162–168.

Hurford, A.J. and Hammerschmidt, K. (1985). $^{40}Ar/^{39}Ar$ and K/Ar dating of the Bishop and Fish Canyon Tuffs: calibration ages for fission-track dating standards. *Chemical Geology (Isotope Geoscience Section)*, **58**, 23–32.

Ivanovich, M. (1982). The phenomenon of radioactivity. *In*: Ivanovich, M. and Harmon, R.S. (eds), *Uranium Series Disequilibrium: Applications to Environmental Problems*, pp. 1–32. Clarendon Press, Oxford.

Ivanovich, M., Ku, T.-L., Harmon, R.S. and Smart, P.L. (1984). Uranium Series Intercomparison Project (USIP): *Nuclear Instruments and Methods in Physics Research*, **223**, 466–471.

Kaufman, A., Broecker, W.S., Ku, T.-L. and Thurber, D.L. (1971). The status of U-series methods of mollusk dating. *Geochimica et Cosmochimica Acta*, **35**, 1155–1181.

Kennedy, G.L. (1978). *Pleistocene paleoecology, zoogeography, and geochronology of marine invertebrate faunas of the Pacific Northwest coast (San Francisco Bay to Puget Sound)*. Ph.D. Thesis, Davis, University of California, 824 pp.

Kennedy, G.L., Lajoie, K.R. and Wehmiller, J.F. (1982). Aminostratigraphy and faunal correlations of late Quaternary marine terraces, Pacific Coast, USA. *Nature*, **299**, 545–547.

Kern, J.P. (1977). Origin and history of upper Pleistocene marine terraces, San Diego, California. *Geological Society of America Bulletin*, **88**, 1553–1566.

Ku, T.-L. (1976). The uranium-series methods of age determination. *Annual Review of Earth and Planetary Science Letters*, **4**, 347–379.

Ku, T.-L. and Kern, J.P. (1974). Uranium-series age of the upper Pleistocene Nestor terrace, San Diego, California. *Geological Society of America Bulletin*, **85**, 1713–1716.

Ku, T.-L., Kimmel, M.A., Easton, W.H. and O'Neil, T.J. (1974). Eustatic sea level 120,000 years ago on Oahu, Hawaii. *Science*, **183**, 959–962.

Lajoie, K.R. (1986). Coastal tectonics. *In*: *Active Tectonics*, pp. 95–125. Washington, D.C., National Research Council, National Academy Press.

Lajoie, K.R., Kern, J.P., Wehmiller, J.F., Kennedy, G.L., Mathieson, S.A., Sarna-Wojcicki, A.M., Yerkes, R.F. and McCrory, P.A. (1979). Quaternary marine shorelines and crustal deformation, San Diego to Santa Barbara, California. *In*: Abbot, P.L. (ed.), *Geological Excursions in the Southern California Area*, pp. 3–15. Department of Geological Sciences, San Diego State University, San Diego.

Ludwig, K.R. (1979). A program in Hewlett-Packard BASIC for X–Y plotting and line-fitting of isotopic and other data. *U.S. Geological Survey Open-File Report, 79–1641*, 28 pp.

Ludwig, K.R. (1980). Calculation of uncertainties of U–Pb isotopic data. *Earth and Planetary Science Letters*, **46**, 212–220.

Machette, M.N., Rosholt, J.N. and Bush, C.A. (1986). Uranium-trend ages of Quaternary deposits along the Colorado River, Grand Canyon National Park, Arizona. *Geological Society of America Abstracts with Programs*, **18**, 393.

McLaughlin, R.J., Lajoie, K.R., Sorg, D.H., Morrison, S.D. and Wolfe, J.A. (1983). Tectonic uplift of a middle Wisconsin marine platform near the Mendocino triple junction, California. *Geology*, **11**, 35–39.

Mankinen, E.A. and Dalrymple, G.B. (1979). Revised geomagnetic polarity time scale for the interval 0–5 m.y. B.P. *Journal of Geophysical Research*, **84**, 615–626.

Muhs, D.R. (1982). A soil chronosequence on Quaternary marine terraces, San Clemente Island, California. *Geoderma*, **28**, 257–283.

Muhs, D.R. (1983a). Quaternary sea-level events on northern San Clemente Island, California. *Quaternary Research*, **20**, 322–341.

Muhs, D.R. (1983b). Airborne dust fall on the California Channel Islands, U.S.A. *Journal of Arid Environments*, **6**, 223–238.

Muhs, D.R. (1985). Amino acid age estimates of marine terraces and sea levels on San Nicolas Island, California. *Geology*, **13**, 58–61.

Muhs, D.R. (1987). Geomorphic processes in the Pacific coast and mountain system of southern California. *In*: Graf, W.L. (ed.), *Geomorphic Systems of North America*. Boulder, Colorado, Geological Society of America, Centennial Special Volume 2, pp. 560–570.

Muhs, D.R. and Kennedy, G.L. (1985). An evaluation of uranium-series dating of fossil echinoids from southern California Pleistocene marine terraces. *Marine Geology*, **69**, 187–193.

Muhs, D.R. and Kyser, T.K. (1987). Stable isotope compositions of fossil mollusks from southern California: evidence for a cool last interglacial ocean. *Geology*, **15**, 119–122.

Muhs, D.R. and Rosholt, J.N. (1984). Ages of marine terraces on the Palos Verdes Hills, California, by amino acid and uranium-trend dating. *Geological Society of America Abstracts with Programs*, **16** (6), 603.

Muhs, D.R. and Szabo, B.J. (1982). Uranium-series age of the Eel Point terrace, San Clemente Island, California. *Geology*, **10**, 23–26.

Muhs, D.R., Kennedy, G.L. and Miller, G.H. (1987). New uranium-series ages of marine terraces and late Quaternary sea level history, San Nicolas Island, California. *Geological Society of America Abstracts with Programs*, **19** (7), 780–781.

Omura, A., Emerson, W.K. and Ku, T.-L. (1979). Uranium-series ages of echinoids and corals from the upper Pleistocene Magdalena terrace, Baja California Sur, Mexico. *Nautilus*, **94**, 184–189.

Pierce, K.L. (1979). History and dynamics of glaciation in the northern Yellowstone National Park area. *U.S. Geological Survey Professional Paper 729–F*, pp. F1–F90.

Rockwell, T.K., Wilson, S., Hatch, M.E., Kennedy, G.L. and Muhs, D.R. (1987). Ages and deformation of marine terraces within the Agua Blanca fault zone, northern Baja California, Mexico. *Geological Society of America Abstracts with Programs*, **19** (6), 444.

Rosholt, J.N. (1980). Uranium-trend dating of Quaternary sediments. *U.S. Geological Survey Open-File Report 80–1087*, 65 pp.

Rosholt, J.N. (1984). Radioisotope dilution analyses of geologic samples using ^{236}U and ^{229}Th. *Nuclear Instruments and Methods in Physics Research*, **223**, 572–576.

Rosholt, J.N. (1985). Uranium-trend systematics for dating Quaternary sediments. *U.S. Geological Survey Open-File Report 85–298*, 48 pp.

Rosholt, J.N. and Szabo, B.J. (1982). Comparison of uranium-series dating of coral and uranium-trend dating of coral-bearing terraces on the U.S. Atlantic coastal plain. *Geological Society of America Abstracts with Programs*, **14** (7), 603.

Rosholt, J.N., Doe, B.R. and Tatsumoto, M. (1966). Evolution of the isotopic composition of uranium and thorium in soil profiles. *Geological Society of America Bulletin*, **77**, 987–1004.

Rosholt, J.N., Downs, W.R. and O'Malley, P.A. (1986). Uranium-trend ages of surficial deposits in the central Grand Canyon National Park, Arizona. *Geological Society of America Abstracts with Programs*, **18**, 408.

Rosholt, J.N., Swadley, WC and Bush, C.A. (1988). Uranium-trend dating of fluvial and fan deposits in the Beatty area, Nevada. *In*: Carr, M.D. and Yount, J.C. (eds), *Investigations of a Potential Nuclear Waste Disposal site at Yucca Mountain, Southern Nevada. U.S. Geological Survey Bulletin* **1790**, 129–147.

Rosholt, J.N., Bush, C.A., Shroba, R.R., Pierce, K.L. and Richmond, G.M. (1985a). Uranium-trend dating and calibrations for Quaternary sediments. *U.S. Geological Survey Open-File Report 85–299*, 48 pp.

Rosholt, J.N., Bush, C.A., Carr, W.J., Hoover, D.L., Swadley, WC and Dooley, J.R., Jr (1985b). Uranium-trend dating of Quaternary deposits in the Nevada Test Site area, Nevada and California. *U.S. Geological Survey Open-File Report 85–540*, 72 pp.

Shackleton, N.J. and Opdyke, N.D. (1973). Oxygen isotope and paleomagnetic stratigraphy of equatorial Pacific core V28–238: oxygen isotope temperatures and ice volumes on a 10^5 year and 10^6 year scale. *Quaternary Research*, **3**, 39–55.

Shroba, R.R., Rosholt, J.N. and Madole, R.F. (1983). Uranium-trend dating and soil B horizon properties of till of Bull Lake age, North St. Vrain drainage basin, Front Range, Colorado. *Geological Society of America Abstracts with Programs*, **15** (5), 431.

Szabo, B.J. and Rosholt, J.N. (1982). Surficial continental sediments. *In*: Ivanovich, M. and Harmon, R.S. (eds), *Uranium Series Disequilibrium: Applications to Environmental Problems*, pp. 246–267. Clarendon Press, Oxford.

Szabo, B.J. and Vedder, J.G. (1971). Uranium-series dating of some Pleistocene marine deposits in southern California. *Earth and Planetary Science Letters*, **11**, 283–290.

Vedder, J.G. and Norris, R.M. (1963). Geology of San Nicolas Island, California. *U.S. Geological Survey Professional Paper 369*, 65 pp.

Vedder, J.G., Beyer, L.A., Junger, A., Moore, G.W., Roberts, A.E., Taylor, J.C. and Wagner, H.C. (1974). Preliminary report on the geology of the continental borderland of southern California. *U.S. Geological Survey Map MF–624*.

Wehmiller, J.F. and Belknap, D.F. (1978). Alternative kinetic models for the interpretation of amino acid enantiomeric ratios in fossil mollusks: examples from California, Washington, and Florida. *Quaternary Research*, **9**, 330–348.

Wehmiller, J.F., Lajoie, K.R., Kvenvolden, K.A., Peterson, E., Belknap, D.F., Kennedy, G.L., Addicott, W.O., Vedder, J.G. and Wright, R.W. (1977). Correlation and chronology of Pacific coast marine terrace deposits of continental United States by fossil amino acid stereochemistry — technique evaluation, relative ages, kinetic model ages, and geologic implications. *U.S. Geological Survey Open-File Report 77–680*, 196 pp.

Woodring, W.P., Bramlette, M.N. and Kew, W.W. (1946). Geology and paleontology of Palos Verdes Hills, California. *U.S. Geological Survey Professional Paper 207*, 145 pp.

Woods, A.J. (1980). Geomorphology, deformation, and chronology of marine terraces along the Pacific coast of central Baja California, Mexico. *Quaternary Research*, **13**, 346–364.

York, D. (1969). Least squares fitting of a straight line with correlated errors. *Earth and Planetary Science Letters*, **5**, 320–324.